Published in final edited form as:
Transl Stroke Res. 2011 October 28; 3(1): 76–83. doi:10.1007/s12975-011-0110-4.

Defining an Acidosis-Based Ischemic Penumbra from pH-Weighted MRI

Jinyuan Zhou[1,2,*] and **Peter C.M. van Zijl**[1,2,*]

[1]Division of MRI Research, Department of Radiology and Radiological Sciences, Johns Hopkins University School of Medicine, Baltimore, MD 21287, USA

[2]F.M. Kirby Research Center for Functional Brain Imaging, Kennedy Krieger Institute, Baltimore, MD 21205, USA

Abstract

It has been proposed that the spatial mismatch between deficits on perfusion-weighted imaging (PWI) and diffusion-weighted imaging (DWI) in MRI can be used to decide regarding thrombolytic treatment in acute stroke. However, uncertainty remains about the meaning and reversibility of the perfusion deficit and even part of the diffusion deficit. Thus, there remains a need for continued development of imaging technology that can better define a potentially salvageable ischemic area at risk of infarction. Amide proton transfer (APT) imaging is a novel MRI method that can map tissue pH changes, thus providing the potential to separate the PWI/DWI mismatch into an acidosis-based penumbra and a zone of benign oligemia. In this totally noninvasive method, the pH dependence of the chemical exchange between amide protons in endogenous proteins and peptides and water protons is exploited. Early results in animal models of ischemia show promise to derive an acidosis penumbra. Possible translation to the clinic and hurdles standing in the way of achieving this are discussed.

Keywords

Penumbra; Acidosis; Ischemic threshold; Stroke; Ischemia; Area at risk of infarction; Salvageable tissue; Perfusion/diffusion mismatch; APT; pH imaging; MRI

Introduction

Stroke is the second most frequent cause of mortality worldwide [1]. Thrombolysis treatment of ischemic patients can increase survival and reduce disability, but early intervention is key to successful therapeutic outcome [2,3]. To determine whether treatment will be beneficial, there is a need for advanced diagnostics that can identify the presence of an area of salvageable tissue at risk of infarction. Such an area is often described using the concept of an ischemic penumbra, first suggested for electrically dysfunctional tissue by Astrup et al. [4], and further developed in terms of imaging-based penumbras by several others [5–7]. The penumbra is defined as a tissue region that is functionally impaired and at risk of infarction. “Penumbra” is used because this region generally (but not always) surrounds an area of irreversible damage, but “salvageable tissue” is a more precise description. To evaluate the presence of such tissue in the acute stroke setting it is necessary to have imaging technology that can rapidly and specifically assess brain perfusion and

*Address correspondence to: Jinyuan Zhou, Ph.D. or Peter van Zijl, Ph.D., Division of MRI Research, Department of Radiology, Johns Hopkins University School of Medicine, 600 N. Wolfe Street, Park 336, Baltimore, MD 21287, Phone: (410) 955-7491, Fax: (410) 614-1977, jzhou@mri.jhu.edu, pvanzijl@mri.jhu.edu.

metabolic status. While CT remains the mainstay due to its ease of use for ruling out hemorrhage, MRI and PET are more versatile. Of these latter two, MRI is more readily available and easy to repeat because no ionizing radiation is used. Large-vessel and small-vessel perfusion can be assessed using MR angiography (MRA) and dynamic contrast imaging (perfusion-weighted imaging or PWI), respectively [8]. In addition, T_2*-weighted MRI is suitable to distinguish regions of hemorrhage, a crucial first step in the stroke exam. Diffusion-weighted imaging (DWI) provides information about cellular water shifts and anoxic cell membrane depolarization [9].

In cases of ischemic stroke, it has been proposed to define an MRI penumbra in terms of the mismatch between PWI and DWI abnormalities [10–14] and several trials are underway to test this hypothesis. The two largest trials are DEFUSE [15] and EPITHET [16]. Of these, the DEFUSE study was observational, i.e., all patients received tissue plasminogen activator (tPA) regardless of mismatch. The results show that the PWI/DWI mismatch would be useful for selecting patients who could potentially benefit from early reperfusion [15]. The EPITHET was also a prospective study, but different from DEFUSE in that it was a randomized placebo controlled trial. They failed to meet the primary endpoint of patients with mismatch doing better, but this was later judged to be related to the use of a perfusion timing threshold that was too low. The current EXTEND trial (clinicaltrials.gov) is basically the next EPITHET, but now with proper perfusion timing threshold. Two other trials, RESCUE and DEFUSE2 (clinicaltrials.org) to evaluate the PWI/DWI mismatch potential are also ongoing. Thus, conclusive evidence for the PWI/DWI mismatch hypothesis as a marker for threatened tissue is still being pursued, but the prospects are promising.

Contrary to earlier beliefs that the area of a diffusion deficit in the image is homogeneous and progresses to infarction, recent data have shown metabolic heterogeneity within this zone and that such regions can, at least partially, recover [17,18]. In addition, the area of perfusion/diffusion mismatch is heterogeneous from a flow point of view and may contain regions of benign oligemia that may recover without treatment. Measurement of the mean transit time (MTT), time-to-peak (TTP), time-to-peak of the impulse response (Tmax), and first moment transit time (FMT) of the contrast bolus used for PWI provides an important indicator of the severity of the deficit [19–22], but differences between data analysis approaches (inclusion of arterial input function or not) and the setting of thresholds for such timing parameters affect the size of the penumbra and the correlation with correctness of outcome prediction. Due to the high risk of thrombolytic treatment (hemorrhage) and the uncertainty about the meaning and reversibility of the perfusion deficit and even part of the diffusion deficit, the continued development of novel imaging technology that can shed light on these issues is needed. As such, it is useful to discuss which MR parameters are affected during ischemia.

Ischemic Thresholds and MR

Figure 1 shows a simplified overview of the approximate neurologic ischemic flow thresholds (Fig. 1a) as previously provided by Hossmann [7] and their relationship to some MR parameters (Fig. 1b). When flow reduces below normal, protein synthesis starts to be affected, but metabolism is still normal (benign oligemia). The next stage of chemical change occurs between 35–23 ml/100g/min, where oxidative glucose metabolism is impaired, leading to anaerobic glucose metabolism (lactate formation) and, below about 28–30 ml/100g/min, to tissue acidosis (pH drop). Below 23 ml/100g/min, this energy crisis leads to functional disturbances, such as suppression of EEG, evoked potentials and unit activity. Neurological studies suggest reversible hemiparalysis at flows of about 23 ml/100g/min and irreversible paralysis below 17–18 ml/100g/min. Classically [4], this intermediate zone is referred to as the ischemic penumbra where neuronal function is interrupted but the

ion gradients are still maintained. Finally, at flow rates between 10 and 15 ml/100g/min, anoxic depolarization occurs, leading to major shifts in intracellular sodium, potassium, water, and calcium. Although reversible changes in water shifts have been measured after membrane failure [23,24], as confirmed by recent clinical results, anoxic depolarization often leads to infarction, except for very short ischemic durations. Fig. 1 indicates that the PWI/DWI mismatch includes areas of benign oligemia and that a potentially more useful parameter to assess risk of infarction is pH, which can provide information on tissue acidosis. In principle, ^{1}H MR spectroscopy (MRS) can be used to assess lactate and ^{31}P MRS to asses pH and impaired energy metabolism [25]. However, MRS is time consuming and insensitive (low spatial resolution) and generally not practical in the acute clinical stage. Fortunately, it has recently become possible to perform pH-sensitive imaging by employing the properties of exchangeable amide protons in mobile tissue peptides and proteins [26]. In this brief review we outline the principles of this new amide proton transfer (APT) methodology that can be used to provide an acidosis-based imaging penumbra based on the difference in area affected by pH changes and diffusion changes and a second “penumbra” for benign oligemia. This principle is illustrated in Fig. 1c.

pH-Sensitive MRI Using APT Imaging

Amide protons (NH) in the backbone of solute proteins interact with water protons through chemical exchange (Fig. 2a). The exchange rate (k) of these protons is very pH dependent, and typically decreases ten-fold per unit of pH drop [27,28]. It has been shown that the amide protons of cellular proteins and peptides are detectable in the in vivo proton MR spectrum [26,29,30]. They appear as a broad peak consisting of multiple resonances at a frequency of around 8.25 ppm (Fig. 2b) for which the exchange properties and sensitivity to tissue pH could be confirmed [29]. However, the concentration of cellular mobile proteins and peptides is in the micro-millimolar range and MRS is not sensitive enough for fast detection. Fortunately, a new method called chemical exchange saturation transfer (CEST) imaging has become available that allows detection of the exchangeable protons through the water signal [31,32]. In this approach, the exchangeable protons are saturated (signal erased) at their MR frequency and this saturation is transferred to water. Detection of the effect of mM concentration protons on the water resonance (~110 M protons) would normally not be feasible, but the combined effect of continuous saturation and exchange in which saturated solute protons are replaced by unsaturated water protons allows sensitivity enhancements of 100–1000 fold [31,33]. These CEST effects can be detected using magnetization transfer (MT) spectroscopy in which a so-called Z-spectrum is acquired displaying the water signal attenuation (S_{sat}/S_0) as a function of irradiation frequency over the proton spectrum (Fig. 2c). In such Z-spectra, the proton frequencies are conventionally referenced with respect to the water signal (around 4.75 ppm in the proton spectrum) and new frequencies are assigned to be 0 ppm for water and 3.5 ppm for the amide protons.

We previously named the endogenous CEST effect between amide protons and water the “amide proton transfer” or “APT” effect [26], not to be confused with the biochemical ATP. As can be seen from Fig. 2c, it is not easy to demonstrate APT effects on water signal in tissue due to several confounding MRI phenomena. First, there is a large MT effect [34,35] between solid-like macromolecular structures and cellular water. Secondly, there is direct saturation (DS) of water protons when irradiating near the water signal. However, a small APT effect can be seen in vivo around 3.5 ppm from water, which disappears during cardiac arrest (Fig. 2c). In an effort to remove MT and DS effects, it is custom to perform a so-called MT ratio ($MTR = 1 - S_{sat}/S_0$) asymmetry analysis with respect to the water signal, allowing the in vivo detection of small APT effects (amide proton transfer ratio or APTR). The effect of ischemia on such exchangeable resonances is illustrated in Fig. 3a, showing

that the removal of the MT/DS effects is not perfect in normal brain. Thus, the calculated asymmetry at 3.5 ppm has multiple contributions:

$$MTR_{asym}(3.5ppm)=MTR(+3.5ppm)-MTR(-3.5ppm)=APTR+MTR'_{asym}(3.5ppm), \quad (1)$$

in which APTR is the MTR difference due to the APT effect and an additional term is added to account for remaining asymmetries. In the example in Fig 3a, reduced $MTR_{asym}(3.5ppm)$ is found upon cardiac arrest, which can be attributed to pH reduction causing slower exchange. Notice that even though these APT effects are small (several percent on the water signal), they correspond to a detection sensitivity of molar concentration. By comparing the postmortem and in vivo asymmetries, Zhou et al. [26] were able to determine the change in APTR. Measurement of the in vivo and postmortem pH values and proton exchange rates with ^{31}P and ^{1}H spectroscopy, respectively, allowed calibration of the APTR change in terms of pH by assuming base-catalyzed exchange in the physiological pH range, which is known to be the case for most amide protons. The APTR could be determined to be [26]:

$$APTR=5.73\times 10^{pH-9.4}. \quad (2)$$

This equation indicates that the sensitivity for measuring pH changes in the physiological range (pH 6.5–7.5) is quite good, giving an APTR reduction of 65% between normal (pH ~7.11) and postmortem (pH ~6.66) brain tissue. In vivo during ischemia, depending on the continued delivery of glucose substrate or not, even lower pH values are possible. In the case of stroke, the MTR_{asym} (3.5ppm) images calculated from Eq. (1) are called the pH-weighted (pHW) images (pHWI).

pH Imaging of Focal Brain Ischemia in Rats

Zhou et al. [26] subsequently used APT to study a permanent middle cerebral artery (MCAO) model in the rat brain (n = 7). Interestingly, for this ischemia model, the change in the asymmetry spectrum between the ischemic area and contralateral was very similar to the postmortem/in vivo change (Figs. 3a and b). Using Eq. (2), an absolute pH image could be generated (Fig. 3c), correctly outlining the ischemic area in the caudate nucleus, a region commonly affected by infarction following MCAO. Ischemia was confirmed by DWI and histology, acquired 8 hours later. No infarct was visible on the T_2-weighted (T_2W) image. The average ischemic pH was 6.52 ± 0.32 (n = 7). It is important to note that APTR decreases in ischemic lesion, which is opposite to high grade tumors where APTR is enhanced due to increases in protein content [36,37].

Following this initial study, APT-based pH imaging has been applied to brain ischemia in rats following MCAO by several investigators [38–41]. First, we investigated the possibility of using the APT approach to detect a separate pH-based acidosis penumbra [41]. Adult rats (n = 21) with permanent MCAO were studied using multi-parametric MRI over the first 3.5 hrs post-occlusion. Endpoint was the stroke area defined by T_2 hyperintensity at 24 hrs. The experiment was designed to minimize the occlusion and a diffusion/perfusion mismatch was observed in most rats (18/21), as reported previously [42]. Interestingly, several animals showed negligible apparent diffusion coefficient (ADC) effects in the hyperacute period, despite the presence of perfusion and pH effects (Fig. 4a), confirming that pH changes occur before ADC changes as expected from the ischemic flow thresholds (Fig. 1b). In this particular animal, the pH-deficit at 0.5 hr was much larger than at later time points. We tentatively attribute this to rapid accumulation of lactate in this area at onset when glucose is still available, followed by diffusion of lactate out of this area reducing its size. The group results (Fig. 4b) showed that areas of reduced pH were always larger than or equal to ADC deficits, and smaller than or equal to perfusion deficits in the acute phase for all rats.

Moreover, pH deficits during this phase coincided with the resulting infarct area at the endpoint. These data suggest that the hypoperfused area showing a decrease in pH without ADC abnormality corresponds to the ischemic acidosis penumbra, while the hypoperfused region at normal pH corresponds to benign oligaemia. To illustrate this principle, the different ischemic zones outlined in Fig. 1c were drawn for two animals in Fig. 4c, which could be accomplished using the experimental ADC, pHW and cerebral blood flow (CBF) data. These first results showed that APT-based pH MRI can provide information complementary to perfusion imaging and diffusion imaging in the delineation of ischemic tissue. Sun et al. subsequently performed such experiments using multi-slice acquisition in rats allowing a three-dimensional (3D) pH-based penumbra to be visualized [40]. Jokivarsi et al. [38] measured intracellular pH changes in rat brain tissue during and after MCAO using APT imaging and compared the results quantified by APTR and cerebral lactate concentrations (measured from proton MR spectroscopy). According to the APTR-pH relationship calibrated by Zhou et al. [26] (namely, Eq. (2)), an APTR drop corresponding to an acidification from pH = 7.12 ± 0.06 to 6.79 ± 0.19 (n = 12) was found. Intracellular pH estimated from the lactate concentration was 6.31 ± 0.23 in the lesion. One possible explanation for this small discrepancy is that the calibrated APTR-pH relationship may not be the same at different research centers because the APT technique is not standardized at this time. Another may be the fact that APTR is thought to be intracellular, while lactate is both intra- and extracellular. The lactate-pH correlation used in [43] was based on tissue lactate content. Although the two methods disagreed in terms of the size of the changes, APTR and lactate concentration nevertheless showed a strong correlation during MCAO [38]. This study further showed that APTR returned slowly toward the values determined in the contralateral hemisphere post-ischemia, while ADC did not. This is somewhat puzzling, but may simply indicate pH returning to normal due to buffering of the tissue while the cells are still depolarized and lactate is still produced, in line with other studies [44]. In their second study, Joksivari et al. [39] evaluated only APTR changes post-reperfusion after 60–65 min of MCAO, similarly showing continued (but reduced) acidosis in areas with depolarized cells destined to infarction.

Potential for pH Imaging of Acute Stroke in Humans

The ultimate goal for APT imaging is its use in a clinical setting. However, the technology is complicated and current human APT imaging protocols are not yet optimized [45–49]. Several issues need to be addressed, including proper standardization of normal tissue contrast depending on radiofrequency (RF) power and length used for the saturation experiment, automated correction for inhomogeneities in the static magnetic field (B_0) and the RF field (B_1), fast whole-brain multi-slice or 3D acquisition, and removal of interfering MT/DS contrast. The APT approach has been successfully implemented in some first clinical single-slice studies for the assessment of brain [50,51] and prostate [52] cancers. In these studies, the approach used there for standardization was to choose the RF power and length to accomplish a zero $MTR_{asym}(3.5ppm)$ in normal tissue, allowing increases in protein content in tumors to be directly visualized. When using a similar approach in a preliminary study on a subacute stroke patient [48], a reduction in APTR was found in most infracted brain zone as identified with flow-attenuated inversion recovery (FLAIR) imaging (Fig. 5). This shows promise for the technique in the future, but hyperacute patients without T_2-based changes will need to be studied to confirm this.

APT studies require acquisition of a B_0 field reference map to correct for different water reference frequencies in voxels in different spatial areas to allow for proper calculation of the $MTR_{asym}(3.5ppm)$ image. The reason for this is that the slightest shift in the steep DS curve (Fig. 2c) can drastically change the appearance of the asymmetry map. Corrections can be done by acquiring the full Z-spectrum and frequency shifting each voxel, fast

approaches for which are being developed [53,54]. One reason that clinical applications of APT have remained limited mainly to single-slice acquisition is that the APT experimental parameters are often constrained by scanner hardware requirements, particularly with respect to amplifier duty cycle, and specific absorption rate (SAR) guidelines. However, APT imaging has recently been extended to multiple slices [55–57], already allowing acquisition of 30 slices in about 11 min with sufficient sensitivity [57]. Faster methods will probably be developed.

Conclusions

APT-based pH imaging is a novel noninvasive MRI technology that employs amide protons of endogenous proteins and peptides to image tissue acidosis via the bulk water signal. This approach has the potential to separate the PWI/DWI mismatch into zones of benign oligemia and an acidosis penumbra. Early results in ischemic animal models are promising, but more developments are needed to provide a multi-slice technique ready for fast acute stroke imaging in the clinic.

Acknowledgments

We are grateful to Dr. Ona Wu (MGH) for suggestions with the manuscript. This study was supported in part by grants from NIH (EB009112, EB009731, EB015032, and RR015241).

References

1. World Health Organization. http://gamapserver.who.int/gho/interactive_charts/mbd/cod_2008/graph.html
2. Donnan GA, Baron JC, Ma H, Davis SM. Penumbral selection of patients for trials of acute stroke therapy. Lancet Neurol. 2009; 8(3):261–269. [PubMed: 19233036]
3. Wintermark M, Albers GW, Alexandrov AV, Alger JR, Bammer R, Baron JC, et al. Acute stroke imaging research roadmap. Stroke. 2008; 39(5):1621–1628. [PubMed: 18403743]
4. Astrup, J. Thresholds of cerebral ischemia. In: Schmiedek, P., editor. Microsurgery for stroke. Berlin: Springer; 1976. p. 16-21.
5. Baron JC, Marchal G. Ischemic core and penumbra in human stroke. Stroke. 1999; 30(5):1150–1153. [PubMed: 10229761]
6. Heiss WD. The concept of the penumbra: can it be translated to stroke management? Int J Stroke. 2010; 5(4):290–295. [PubMed: 20636712]
7. Hossmann KA. Viability thresholds and the penumbra of focal ischemia. Ann Neurol. 1994; 36(4): 557–565. [PubMed: 7944288]
8. Moseley ME, Sevick R, Wendland MF, White DL, Mintorovitch J, Asgari HS, et al. Ultrafast magnetic resonance imaging: diffusion and perfusion. Can Assoc Radiol J. 1991; 42(1):31–38. [PubMed: 2001526]
9. Moseley ME, Mintorovitch J, Cohen Y, Asgari HS, Derugin N, Norman D, et al. Early detection of ischemic injury: comparison of spectroscopy, diffusion-, T2-, and magnetic susceptibility-weighted MRI in cats. Acta Neurochir Suppl (Wien). 1990; 51:207–209. [PubMed: 2089896]
10. Neumann-Haefelin T, Wittsack HJ, Wenserski F, Siebler M, Seitz RJ, Modder U, et al. Diffusion- and perfusion-weighted MRI - The DWI/PWI mismatch region in acute stroke. Stroke. 1999; 30(8):1591–1597. [PubMed: 10436106]
11. Schaefer PW, Grant PE, Gonzalez RG. Diffusion-weighted MR imaging of the brain. Radiology. 2000; 217(2):331–345. [PubMed: 11058626]
12. Schellinger PD, Jansen O, Fiebach JB, Heiland S, Steiner T, Schwab SF, et al. Monitoring intravenous recombinant tissue plasminogen activator thrombolysis for acute ischemic stroke with diffusion and perfusion MRI. Stroke. 2000; 31(6):1318–1328. [PubMed: 10835451]

13. Schlaug G, Benfield A, Baird AE, Siewert B, Lovblad KO, Parker RA, et al. The ischemic penumbra - Operationally defined by diffusion and perfusion MRI. Neurology. 1999; 53(7):1528–1537. [PubMed: 10534263]
14. Wu O, Koroshetz WJ, Ostergaard L, Buonanno FS, Copen WA, Gonzalez RG, et al. Predicting tissue outcome in acute human cerebral ischemia using combined diffusion- and perfusion-weighted MR imaging. Stroke. 2001; 32(4):933–942. [PubMed: 11283394]
15. Albers GW, Thijs VN, Wechsle L, Kemp S, Schlaug G, Skalabrin E, et al. Magnetic resonance imaging profiles predict clinical response to early reperfusion: The diffusion and perfusion imaging evaluation for understanding stroke evolution (DEFUSE) study. Ann Neurology. 2006; 60(5):508–517.
16. Davis SM, Donnan GA, Parsons MW, Levi C, Butcher KS, Peeters A, et al. Effects of alteplase beyond 3 h after stroke in the echoplanar imaging thrombolytic evaluation trial (EPITHET): A placebo-controlled randomised trial. Lancet Neurol. 2008; 7(4):299–309. [PubMed: 18296121]
17. Kidwell CS, Alger JR, Saver JL. Evolving paradigms in neuroimaging of the ischemic penumbra. Stroke. 2004; 35(11 Suppl 1):2662–2665. [PubMed: 15472112]
18. Nicoli F, Lefur Y, Denis B, Ranjeva JP, Confort-Gouny S, Cozzone PJ. Metabolic counterpart of decreased apparent diffusion coefficient during hyperacute ischemic stroke: a brain proton magnetic resonance spectroscopic imaging study. Stroke. 2003; 34(7):e82–87. [PubMed: 12817104]
19. Butcher KS, Parsons M, MacGregor L, Barber PA, Chalk J, Bladin C, et al. Refining the perfusion-diffusion mismatch hypothesis. Stroke. 2005; 36(6):1153–1159. [PubMed: 15914768]
20. Kakuda W, Lansberg MG, Thijs VN, Kemp SM, Bammer R, Wechsler LR, et al. Optimal definition for PWI/DWI mismatch in acute ischemic stroke patients. J Cereb Blood Flow Metab. 2008; 28(5):887–891. [PubMed: 18183031]
21. Toth G, Albers GW. Use of MRI to estimate the therapeutic window in acute stroke: Is perfusion-weighted imaging/diffusion-weighted imaging mismatch an EPITHET for salvageable ischemic brain tissue? Stroke. 2009; 40(1):333–335. [PubMed: 18845795]
22. Wu O, Ostergaard L, Koroshetz WJ, Schwamm LH, O'Donnell J, Schaefer PW, et al. Effects of tracer arrival time on flow estimates in MR perfusion-weighted imaging. Magn Reson Med. 2003; 50(4):856–864. [PubMed: 14523973]
23. Davis D, Ulatowski J, Eleff S, Izuta M, Mori S, Shungu D, et al. Rapid monitoring of changes in water diffusion coefficients during reversible ischemia in cat and rat brain. Magn Reson Med. 1994; 31(4):454–460. [PubMed: 8208123]
24. Minematsu K, Li L, Sotak CH, Davis MA, Fisher M. Reversible focal ischemic injury demonstrated by diffusion-weighted magnetic resonance imaging in rats. Stroke. 1992; 23(9): 1304–1310. discussion 1310–1301. [PubMed: 1519287]
25. Crockard HA, Gadian DG, Frackowiak RS, Proctor E, Allen K, Williams SR, et al. Acute cerebral ischaemia: concurrent changes in cerebral blood flow, energy metabolites, pH, and lactate measured with hydrogen clearance and 31P and 1H nuclear magnetic resonance spectroscopy. II. Changes during ischaemia. J Cereb Blood Flow Metab. 1987; 7(4):394–402. [PubMed: 3611203]
26. Zhou J, Payen JF, Wilson DA, Traystman RJ, van Zijl PC. Using the amide proton signals of intracellular proteins and peptides to detect pH effects in MRI. Nat Med. 2003; 9(8):1085–1090. [PubMed: 12872167]
27. Englander SW, Downer NW, Teitelbaum H. Hydrogen exchange. Annu Rev Biochem. 1972; 41:903–924. [PubMed: 4563445]
28. Wuthrich, K. NMR of proteins and nucleic acids. New York: John Wiley & Sons; 1986.
29. Mori S, Eleff SM, Pilatus U, Mori N, van Zijl PCM. Proton NMR spectroscopy of solvent-saturable resonance: a new approach to study pH effects *in situ*. Magn Reson Med. 1998; 40:36–42. [PubMed: 9660550]
30. van Zijl PCM, Zhou J, Mori N, Payen J, Mori S. Mechanism of magnetization transfer during on-resonance water saturation. A new approach to detect mobile proteins, peptides, and lipids. Magn Reson Med. 2003; 49:440–449. [PubMed: 12594746]

31. Ward KM, Aletras AH, Balaban RS. A new class of contrast agents for MRI based on proton chemical exchange dependent saturation transfer (CEST). J Magn Reson. 2000; 143:79–87. [PubMed: 10698648]
32. Zhou J, van Zijl PC. Chemical exchange saturation transfer imaging and spectroscopy. Progr NMR Spectr. 2006; 48:109–136.
33. van Zijl PC, Yadav NN. Chemical exchange saturation transfer (CEST): what is in a name and what isn't? Magn Reson Med. 2011; 65(4):927–948. [PubMed: 21337419]
34. Balaban RS, Ceckler TL. Magnetization transfer contrast in magnetic resonance imaging. Magn Reson Q. 1992; 8:116–137. [PubMed: 1622774]
35. Henkelman RM, Stanisz GJ, Graham SJ. Magnetization transfer in MRI: a review. NMR Biomed. 2001; 14:57–64. [PubMed: 11320533]
36. Zhou J, Lal B, Wilson DA, Laterra J, van Zijl PC. Amide proton transfer (APT) contrast for imaging of brain tumors. Magn Reson Med. 2003; 50(6):1120–1126. [PubMed: 14648559]
37. Zhou J, Tryggestad E, Wen Z, Lal B, Zhou T, Grossman R, et al. Differentiation between glioma and radiation necrosis using molecular magnetic resonance imaging of endogenous proteins and peptides. Nat Med. 2011; 17(1):130–134. [PubMed: 21170048]
38. Jokivarsi KT, Grohn HI, Grohn OH, Kauppinen RA. Proton transfer ratio, lactate, and intracellular pH in acute cerebral ischemia. Magn Reson Med. 2007; 57(4):647–653. [PubMed: 17390356]
39. Jokivarsi KT, Hiltunen Y, Tuunanen PI, Kauppinen RA, Grohn OH. Correlating tissue outcome with quantitative multiparametric MRI of acute cerebral ischemia in rats. J Cereb Blood Flow Metab. 2010; 30(2):415–427. [PubMed: 19904287]
40. Sun PZ, Murata Y, Lu J, Wang X, Lo EH, Sorensen AG. Relaxation-compensated fast multislice amide proton transfer (APT) imaging of acute ischemic stroke. Magn Reson Med. 2008; 59(5): 1175–1182. [PubMed: 18429031]
41. Sun PZ, Zhou J, Sun W, Huang J, van Zijl PC. Detection of the ischemic penumbra using pH-weighted MRI. J Cereb Blood Flow Metab. 2007; 27(6):1129–1136. [PubMed: 17133226]
42. Shen Q, Meng X, Fisher M, Sotak CH, Duong TQ. Pixel-by-pixel spatiotemporal progression of focal ischemia derived using quantitative perfusion and diffusion imaging. J Cereb Blood Flow Metab. 2003; 23:1479–1488. [PubMed: 14663344]
43. Katsura K, Asplund B, Ekholm A, Siesjo BK. Extra- and Intracellular pH in the Brain During Ischaemia, Related to Tissue Lactate Content in Normo- and Hypercapnic rats. Eur J Neurosci. 1992; 4(2):166–176. [PubMed: 12106379]
44. Allen K, Busza AL, Crockard HA, Frackowiak RS, Gadian DG, Proctor E, et al. Acute cerebral ischaemia: concurrent changes in cerebral blood flow, energy metabolites, pH, and lactate measured with hydrogen clearance and 31P and 1H nuclear magnetic resonance spectroscopy. III. Changes following ischaemia. J Cereb Blood Flow Metab. 1988; 8(6):816–821. [PubMed: 3192646]
45. Jones CK, Schlosser MJ, van Zijl PC, Pomper MG, Golay X, Zhou J. Amide proton transfer imaging of human brain tumors at 3T. Magn Reson Med. 2006; 56(3):585–592. [PubMed: 16892186]
46. Schmitt B, Zaiß M, Zhou J, Bachert P. Optimization of pulse train presaturation for CEST imaging in clinical scanners. Magn Reson Med. 2011; 65:1620–1629. [PubMed: 21337418]
47. Sun PZ, Wang E, Cheung JS, Zhang X, Benner T, Sorensen AG. Simulation and optimization of pulsed radio frequency irradiation scheme for chemical exchange saturation transfer (CEST) MRI-demonstration of pH-weighted pulsed-amide proton CEST MRI in an animal model of acute cerebral ischemia. Magn Reson Med. Online: 24 MAR 2011. 10.1002/mrm.22894
48. Zhao X, Wen Z, Huang F, Lu S, Wang X, Hu S, et al. Saturation power dependence of amide proton transfer image contrasts in human brain tumors and strokes at 3 T. Magn Reson Med. Online: 10 MAR 2011. 10.1002/mrm.22891
49. Zhou J. Amide proton transfer imaging of the human brain. Methods Mol Biol. 2011; 711:227–237. [PubMed: 21279604]
50. Wen Z, Hu S, Huang F, Wang X, Guo L, Quan X, et al. MR imaging of high-grade brain tumors using endogenous protein and peptide-based contrast. NeuroImage. 2010; 51(2):616–622. [PubMed: 20188197]

51. Zhou J, Blakeley JO, Hua J, Kim M, Laterra J, Pomper MG, et al. Practical data acquisition method for human brain tumor amide proton transfer (APT) imaging. Magn Reson Med. 2008; 60(4):842–849. [PubMed: 18816868]

52. Jia GA, Abaza R, Williams JD, Zynger DL, Zhou JY, Shah ZK, et al. Amide proton transfer MR imaging of prostate cancer: A preliminary study. J Magn Reson Imaging. 2011; 33(3):647–654. [PubMed: 21563248]

53. Kim M, Gillen J, Landman BA, Zhou J, van Zijl PC. Water saturation shift referencing (WASSR) for chemical exchange saturation transfer (CEST) experiments. Magn Reson Med. 2009; 61(6): 1441–1450. [PubMed: 19358232]

54. Sun PZ, Farrar CT, Sorensen AG. Correction for artifacts induced by B(0) and B(1) field inhomogeneities in pH-sensitive chemical exchange saturation transfer (CEST) imaging. Magn Reson Med. 2007; 58(6):1207–1215. [PubMed: 17969015]

55. Dixon WT, Hancu I, Ratnakar SJ, Sherry AD, Lenkinski RE, Alsop DC. A multislice gradient echo pulse sequence for CEST imaging. Magn Reson Med. 2010; 63(1):253–256. [PubMed: 19918889]

56. Sun PZ, Cheung JS, Wang E, Benner T, Sorensen AG. Fast multislice pH-weighted chemical exchange saturation transfer (CEST) MRI with Unevenly segmented RF irradiation. Magn Reson Med. 2011; 65(2):588–594. [PubMed: 20872859]

57. Zhu H, Jones CK, van Zijl PC, Barker PB, Zhou J. Fast 3D chemical exchange saturation transfer (CEST) imaging of the human brain. Magn Reson Med. 2010; 64(3):638–644. [PubMed: 20632402]

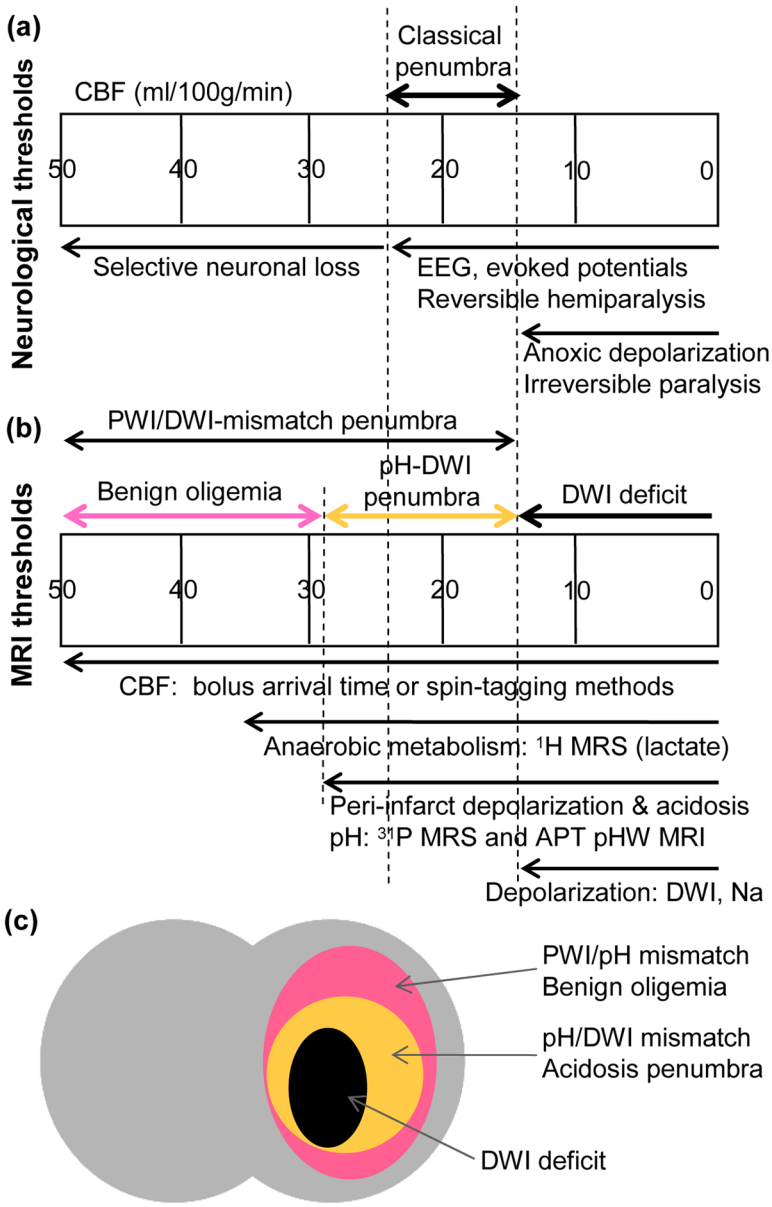

Figure 1.

Simplified depiction of relationships between CBF-based ischemic neurological (**a**) and MRI parameter (**b**) thresholds. Thresholds are approximate, assuming normal CBF of about 50 ml/100g/min, and may shift with time depending on the ischemic duration. (**c**) Parcellation of ischemic area in terms of three zones, a DWI deficit most likely proceeding to infarction, a pH/DWI mismatch region at risk of infarction and a PWI/pH mismatch not at risk.

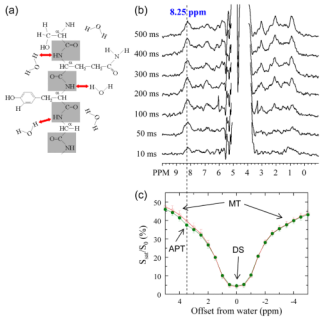

Figure 2.

(**a**) Depiction of exchange interaction between amide protons (NH) in the protein/peptide backbone and water protons. (**b**) Detection of this interaction by water-exchange (WEX) proton NMR via labeling the water signal and watching the amide proton signals (at 8.25 ppm, blue line) appear as a function of waiting time (mixing time T_m). These WEX spectra were obtained in vivo in the rat brain at 4.7 T. (**c**) The opposite process (amide proton to water proton) can be monitored by acquiring a Z-spectrum, in which the ratio of water intensity with saturation (S_{sat}) and without (S_0) is plotted as a function of saturation frequency. In addition to DS (assigned as 0 ppm) and conventional MT effects, an additional saturation can be seen at 8.25 ppm (i.e., 3.5 ppm from water) in vivo (green) but not postmortem (red) due to the reduced pH and lower exchange rate. (Reproduced, with permission, from Zhou J, et al. Nature Med. 2003;9:1085–1090)

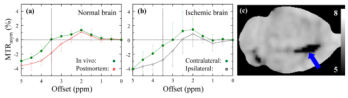

Figure 3.

MTR asymmetry spectra obtained by asymmetry analysis of Z-spectrum with respect to water frequency (right - left) showing combined APT and residual MT effects around 3.5 ppm offset from water. The APTR can be determined by comparing normal and impaired tissue. When comparing the in vivo/postmortem (**a**) and contralateral/ipsilateral (**b**) differences between normal and ischemic brain, they are comparable, indicating similar pH effects. Using a voxel-based calculation, a pure pH image can be calculated (**c**). The caudate nucleus (arrow) shows the largest change. Based on the two-point pH calibration, an average ischemic pH of 6.52 ± 0.32 (n = 7) was found there. (Reproduced, with permission, from Zhou J, et al. Nature Med. 2003;9:1085–1090.)

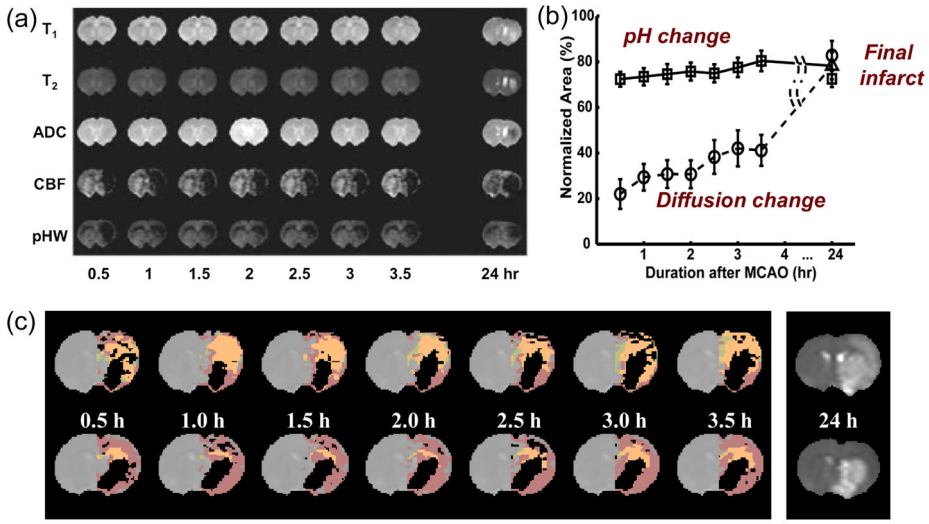

Figure 4.

Multi-parameter MRI as a function of time after permanent MCAO in the rat. (**a**) Example in which no T_1, T_2, and ADC changes were seen, but ischemia was confirmed by hemispheric CBF reduction (obtained using arterial spin labeling) and a pHW deficit measured by APT imaging. Hyperintensity in the T_2 image at 24 hrs gives the final infarction area. (**b**) Group analysis of ischemic volume evolution for 18 rats with perfusion/diffusion mismatch, comparing areas of APT change (pH) and diffusion change as fraction of the perfusion-deficit region. The pHW region predicted well the evolution to infarction. (**c**) Processed images for two other animals showing evolution of pHW deficit (orange) and diffusion deficit (black) with respect to perfusion deficit (purple) as a function of time post-MCAO. The T_2 image at 24 hrs shows final infarction area predicted well by diffusion + pH regions. (Reproduced in part, with permission, from Sun PZ, et al. J Cereb Blood Flow Metab. 2007;27:1129–1136.)

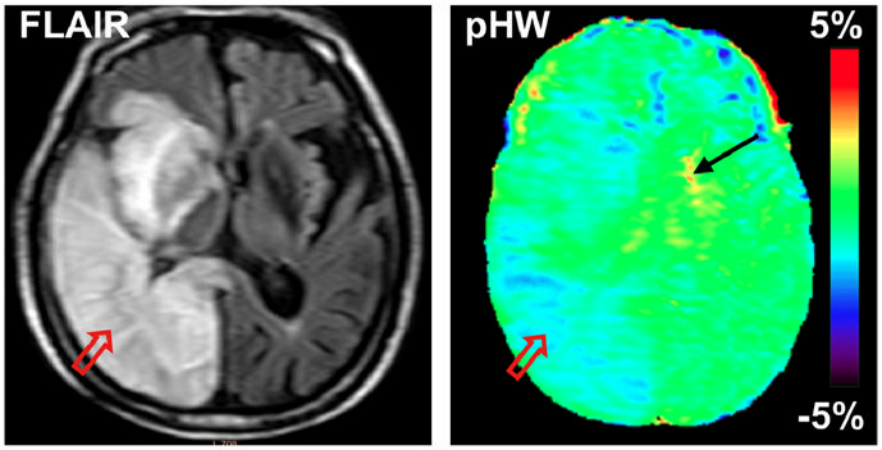

Figure 5.
Conventional and pHW MR images of a patient with stroke at 5 days post-onset. The hyperintense stroke area identified on the FLAIR image (T_2W with CSF suppressed) by the red arrow is hypointense on the pHW image. (Reproduced, with permission, from Zhao X, et al. Magn Reson Med. 2011;65:doi: 10.1002/mrm.22891.)